Chapter-4

Low Profile Conformal Ultra Wideband Absorber

4.1. Introduction

In rapidly evolving landscape of modern IoT and wireless application, there is a huge demand for a low-profile absorber that can integrate with the compact and dynamic requirements of contemporary technologies [111]. In this context, an artifically engineered absorber can provide more effective solution compared to traditional absorber. With the advancement of wireless technology and electronic equipment, design of absorber with wideband performance characteristic is also increasing. In modern era researcher must consider the key factor such as design which can be scalable from lower to higher frequency, independent control on operating band, low profile, and some miniaturized performance while maintaining the conformal characteristic when aiming to create an efficient absorber for practical application. Various types of perfect absorbers [22], [112], [113], wideband absorbers have been reported [32], [37].

However, as discussed in chapter 3, anisotropic geometry is not a good choice for achieving ultra-wideband absorption due to existence of its high cross-polarized reflected component. Therefore, investigation of cross-polarized component is crucial because achieving wideband absorption without significant ohmic or dielectric loss is challenging.

In the literature, various structures have been presented so far to increase the absorption bandwidth by introducing ohmic and dielectric losses. A 3D periodic structure with lumped resistor was presented in [47], [48], with folded resistive patches [114]. By using artificial impedance surface [49], wideband absorption is achieved. However, such approach makes the absorber very thick and complex. Another approach to enhance absorption bandwidth with optimal thickness performance is the utilization of low-pass resistive square patch array [50], [115]. But these are multi-layered structures. Other method to achieve bandwidth enhancement is by tailoring multiple resonances of various resonators [116]. Absorbers with reasonable low profile with wide bandwidth were also presented [51], [52], [117], [118], [119]. Subsequently, to improve the absorption bandwidth, wideband absorbers with dual [53], [54], [84] or multiple resonances [55], [118], [56], [83], [120], [121], [52] were realized.

The advantage of most of these reported absorbers is that the bandwidth performance has improved. However, each resonant frequency cannot be adjusted independently, and hence, the absorber's design flexibility is poor for adapting to a variety of devices . Recently in the literature, a dual stopband FSS was reported [122]. In this work, each resonant frequency, and hence, opearating band can be independently adjusted. The FSS design flexibility was best for adapting to a the variety of devices.

To date, rare studies have comprehensively addressed ultra-wideband performance of low-profile absorbing structures while deliberately controlling each resonance independently.

Motivated by aforementioned discussion, in this chapter, a novel resistive metasurface based absorber is proposed having simultaneous realization of following salient features:

1) Equation based curve printed low profile structure design methodology
2) Independent control on each resonance frequency and hence operating bandwidth
3) Ultra wideband absorption with low cross-polarization
4) Conformality along with some miniaturized absorbing structure performance.

4.2 Design Evolution and Analysis

4.2.1 Design of unit cell as per limiting frequency range

The unit cell geometry of the proposed absorber is illustrated in Fig. 4.1(a). It consists of resistor loaded three serration rings etched on very thin FR-4 substrate (ε_r =4.4

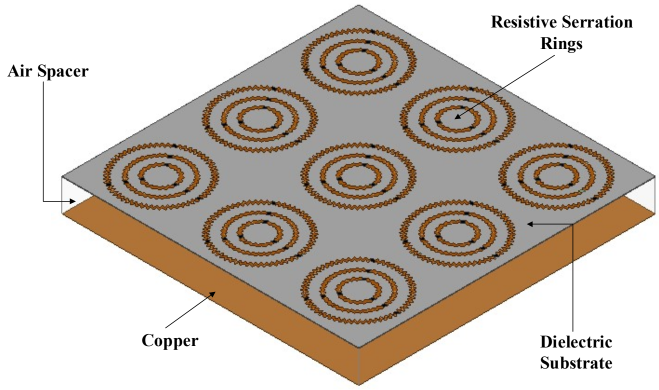

(a)

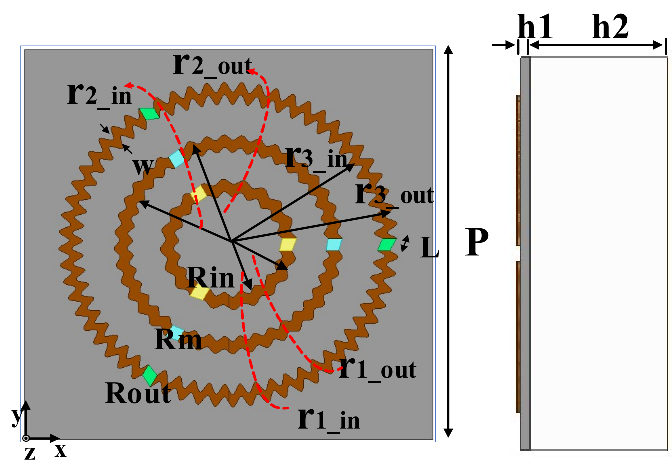

(b) (c)

Fig. 4.1: Illustration of the geometry of proposed absorber. (a) 3-D view of 3 ×3-unit cell (b) Top view of the unit cell (c) Side view of the unit cell.

and tan δ= 0.02). Lumped resistance is employed instead of other resistive additive manufacturing method, such as screen printing technique, to overcome the optimal surface resistance problem [123]. In order to increase the absorption bandwidth, the height between the top resistive layer and the ground plane is initially approximated using the quarter-wavelength condition [124].

To maintain lightweight and conformal characteristic, PMI foam is used as an air spacer. The structure is simulated with master/slave boundaries in *x*- and *y*- directions with Floquet port in *z*- direction using ANSYS HFSS v.19. The design evolution of the structure is presented in Fig. 4.2(a) and 4.2(b).

For the design purpose we have chosen frequency range of interest *X*-, *Ku*- and some portion of the *C*- band. For this objective, we employed the concept of a ring resonator, with its fundamental frequency determined using equation (4.1).

$$f_0 \approx c/\ (2\pi R_{mean.})\sqrt{\varepsilon_{eff}} \tag{4.1}$$

where, εeff is the effective permittivity of metasurface and R_{mean} is the mean radius of the ring [101]. Initially, individually, three rings of different mean radii are used.

To provide comprehensive theoretical framework for our design, we employ parametric equations for each *i*-th serration ring (*i* = 1, 2, 3 is used for Ring 1, Ring 2, and Ring 3, respectively), which are elaborated as follow:

For inner side periphery

$$x(t)=\left[r_{i\_in}+a*\sin(n_i*t)\right]*\cos(t) \tag{4.2}$$

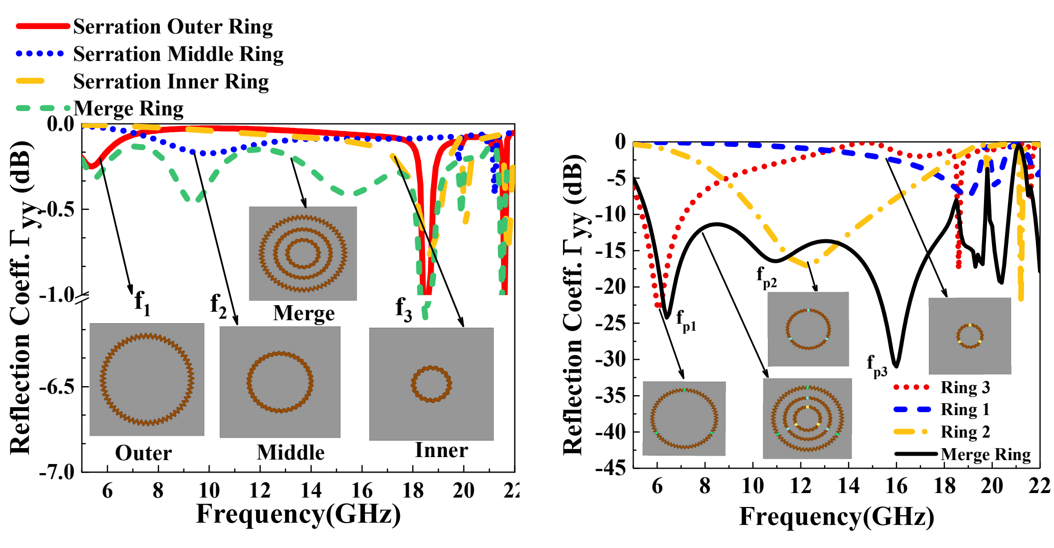

(a) (b)

Fig. 4.2: Reflection coefficient (a) For larger ring, smaller ring with and without sinusoidal periphery. (b) For individual and merge Ring 1, Ring 2, and Ring 3 after embedded with chip resistor.

$$y(t) = \left[r_{i\_in} + a * \sin(n_i * t) \right] * \sin(t)$$

For outer side periphery

$$x(t) = \left[r_{i\_out} + a * \sin(n_i * t) \right] * \cos(t) \quad (4.3)$$

$$y(t) = \left[r_{i\_out} + a * \sin(n_i * t) \right] * \sin(t)$$

where, for *i*-th ring, angular frequency, outer radius, and inner radius are represented by n_i, r_{i_out}, *and* r_{i_in}, respectively, while the maximum amplitude of the outer and inner sinusoidal periphery is represented by *a*.

Among the chosen ring, the larger ring resonates near the lowest frequency f_1 = 5.39 GHz, smaller rings resonate near the higher frequency f_3 = 18.71 GHz, while the third ring resonates at f_2 = 9.88 GHz (where $f_1 < f_2 < f_3$). After that, to obtain the pronounced dip, an ohmic loss is introduced by embedding three lumped resistors at each serration ring, shown in Fig. 4.2(b). Finally, when these individual resistive rings are combined, they form a metasurface unit cell. Optimizing this unit cell for the best absorption performance yields an ultra-wideband response spanning from 5.57 GHz to 18.31 GHz, with three resonant frequencies at f_{p1}= 6.40 GHz, f_{p2}= 10.92 GHz, f_{p3}= 16 GHz. Moreover, a sinusoidal periphery is employed on each ring to increase the length of the current path, resulting in an absorption bandwidth increases from 103.70 % to 106.70 %. Therefore, this periphery has miniaturized the proposed absorbing structure in comparison to a structure without a sinusoidal periphery, as shown in Fig. 4.3.

4.2.2 Parametric analysis

The parametric study of key parameters such as periodicity (*P*), spacer height (h_2), and resistances (inner ring, middle ring, and outer ring R_{in} , R_m, and R_{out}, respectively) are investigated in Fig. 4.4 and Fig. 4.5.

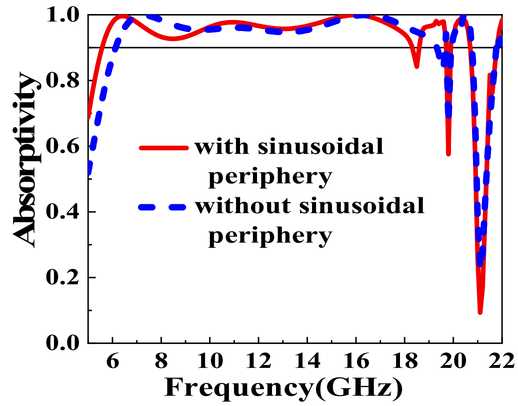

Fig. 4.3: Absorptivity response of the proposed structure with and without sinusoidal periphery.

For best absorption performance, the optimized parameters under fabrication tolerance limit are r_{1_in} = 2.0 mm, r_{1_out} = 2.5 mm, r_{2_in} = 3.75 mm, r_{2_out} = 4.25 mm, r_{3_in} = 5.75 mm, r_{3_out} = 6.25 mm, $w = L$ =0.5 mm, h_1 = 0.1 mm, h_2 = 5 mm, R_{in} = 105 Ω, R_m = 150 Ω, R_{out} = 205 Ω. The angular frequency of sinusoidal periphery of Ring 1, Ring 2 and Ring 3 are n_1 = 20, n_2 = 40, and n_3 = 60, respectively. While the maximum amplitude of the outer and inner sinusoidal periphery is a= 0.1. The design process and the changes in frequency response due to variations in individual resistance, as shown Fig. 4.5 (a), 4.5(b), and 4.5(c), confirm that each resonant frequency is independently controlled by an individual ring. Therefore, absorber design flexibility is best for adopting a variety of devices.

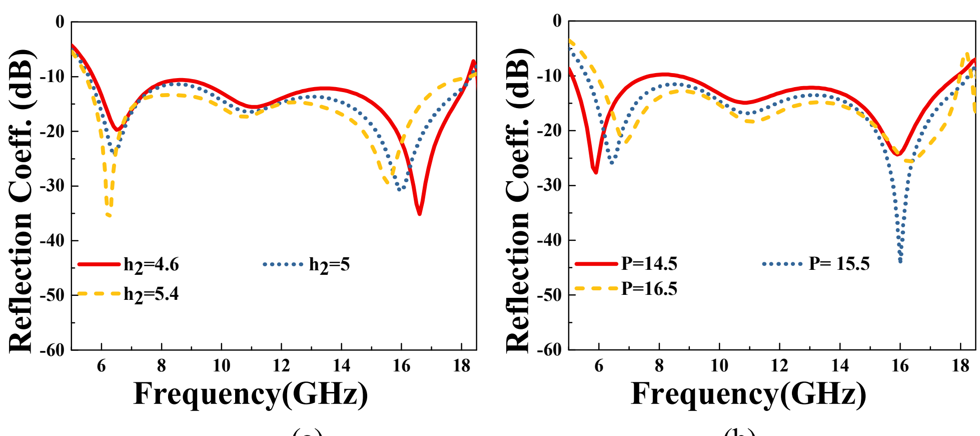

Fig. 4.4 Parametric analysis for reflection coefficient (a) For different values of h_2 (b) periodicity P .

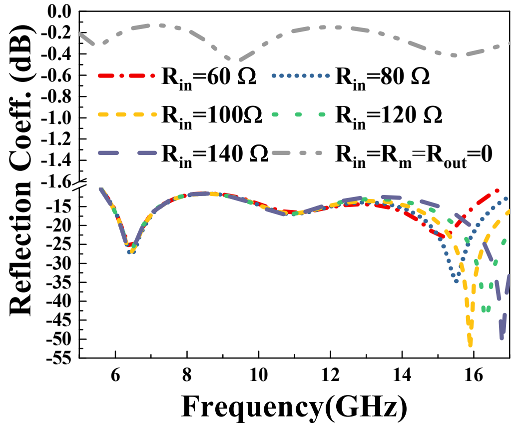

(a)

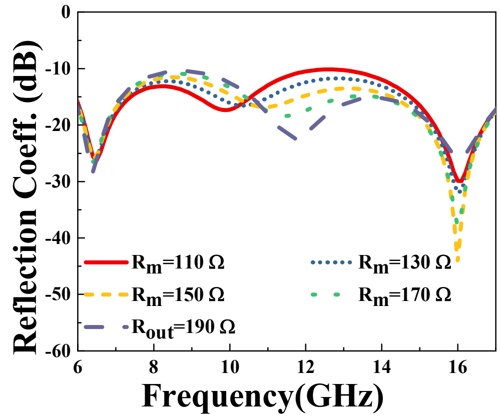

(b)

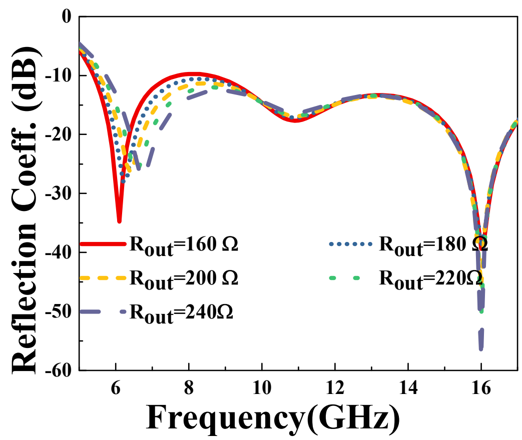

(c)

Fig. 4.5 Reflection Coefficient for (a) different values of R_{in}, when R_m and R_{out} constant (b) different values of R_m, when R_{in} and R_{out} constant (c) (a) different values of R_{out}, when R_{in} and R_m constant.

4.2.3 *Equivalent circuit analysis*

The simplified qualitative equivalent circuit model of the proposed absorber is depicted in Fig. 4.6 (a). In this circuit, each ring can be modeled as an R_N L_N C_N resonator connected in parallel [106], where N=1, 2, 3. R_N is the equivalent losses introduced by each ring, C_N is the equivalent capacitance between adjacent ring element, L_N is the equivalent inductance of each rings. The dielectric substrate and air spacer are modeled with cascaded transmission line sections (Z_{01}, θ_{el1}) and (Z_{02}, θ_{el2},), while the ground plane is represented as a short circuit. The initial value of inductance L_1, L_2, L_3 of the ring is approximated by using a well-defined equation for circular loop [107].

$$L_i(nH)=1.257\times10^{-3}\times r_{i\,mean}\cdot\left[\ln\left(\frac{r_{i\,mean}}{w_i+t_{cu}}\right)+0.078\right].K_g \tag{4.4}$$

where, $r_{i\text{-}mean}$, w_i, t_{cu} are dimension in micrometer and they are mean radius, width and the copper thickness of i-th ring respectively. K_g is the correction factor that accounts for the presence of the ground plane. Since the ring has an increased periphery with respect to a simple annular ring, therefore this inductance formula is used as an initial approximation for the inductance value of each ring of proposed structure.

From Fig. 4.6(b), by utilizing the resonance frequency of each *RLC* arm, the initial value of capacitance C_1 due to higher resonance frequency (ω_3) and capacitance C_2 due to lower resonance frequency (ω_1), and third resonance between these two resonances are determined by using equation (4.5)

$$C_1=\frac{1}{\omega_3^2 L_1}, C_2=\frac{1}{\omega_2^2 L_2}, C_3=\frac{1}{\omega_1^2 L_3} \tag{4.5}$$

Once the initial value of electrical parameters are obtained using above relation, it is later implemented in Advance Design System (ADS) software, where curve fitting technique is used to tune the reflection from the circuit model to full-wave EM simulation to extract the circuit parameter as R_1 = 310.25 Ω, L_1 = 6 nH, C_1 = 1.62 fF, R_2 = 210.45 Ω, L_2 = 8 nH, C_2 = 2.62 fF, R_3 = 350.40 Ω, L_3 = 15.04 nH, C_3 = 41.55 fF.

Fig. 4.6 (c) represent the fair degree of congruence between full wave simulation from HFSS and circuit simulation from ADS software and validates the proposed model.

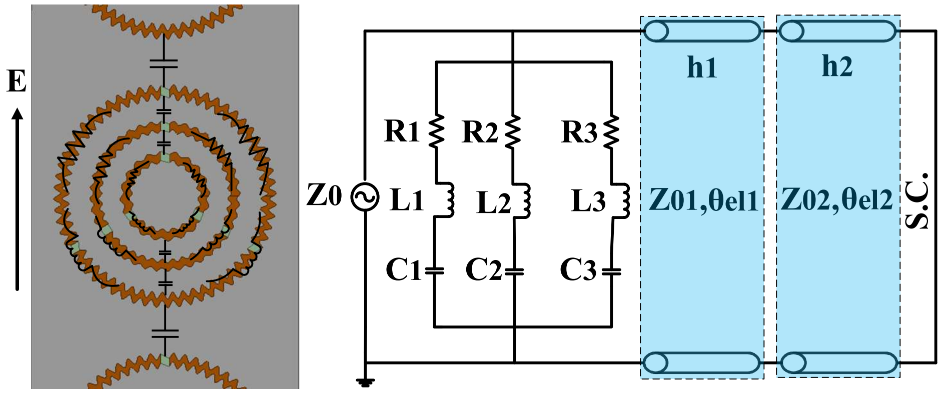

(a) (b)

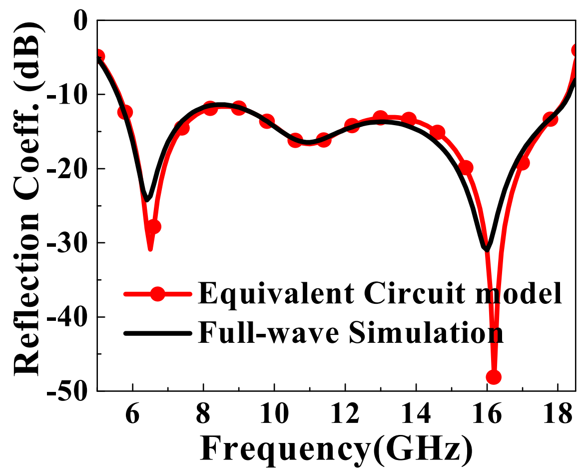

(c)

Fig. 4.6: (a) Conceptual interpretation of Inductive and Capacitive effect on top resistive metasurface (b) Simplified equivalent circuit model of proposed absorber (c) Comparison of equivalent circuit model with HFSS simulated response

4.3 Simulation and Experimental Validation

4.3.1 Simulated performance discussion

The absorptivity of the metal ground absorber for a y (or TE)-polarized incident wave is calculated by [125] $A(\omega)=1-|\Gamma_{yy}(\omega)|^2-|\Gamma_{xy}(\omega)|^2$, where $\Gamma_{xy}(\omega)$, $\Gamma_{xy}(\omega)$ are cross- and co- polarized reflection coefficients. From Fig. 4.7 (a), it can be inferred that co-polarization reflection level is below -10 dB from 5.57 GHz to 18.31 GHz, while due to centro-symmetry of the structure, cross polarization is negligible [89]. Hence, absorptivity spectra are above 90%, from 5.57 GHz to 18.31 GHz as ilustrated in Fig. 4.7 (b).

To gain insights into absorption mechanism, the input impedance of the absorber is plotted in Fig. 4.7(c), from which it can be observed that its imaginary part is near to zero, and the real part is near to free space impedance within the absorption band.

Therefore, there is minimal reflection from the proposed absorbing configuration due to its impedance matching with free space. Moreover, the absorptivity response of the proposed absorber is plotted with and without resistance in Fig. 4.6 (b). From the plot, it can be observed that without resistance, absorptivity is neglible, and hence it confirms that in ultra-wideband absorption, losses in the absorber are predominantly ohmic.

Further performance of the structure is investigated for different polarization angles and different oblique incidences under TE and TM polarizations cases, as shown in

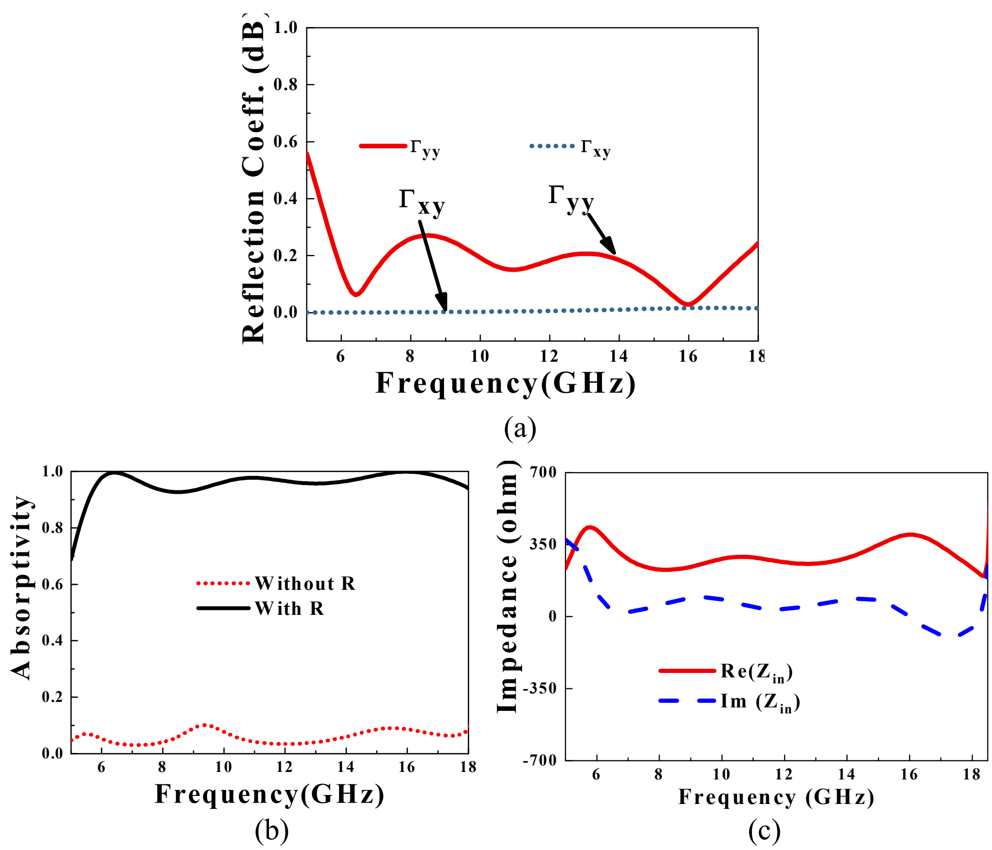

Fig. 4.7 (a) Co- and Cross- polarized reflection coefficient (b) Absorptivity with and without Resistance (c) Impedance characteristic.

Fig. 4.8. Absorptivity response in Fig. 4.8 (a) verifies its polarization-insensitive characteristic. Moreover, the structure gives more than 80% absorptivity and quite stable performance up to a specular angle of 40° within the operating band under both TE and TM polarization cases, as depicted in Fig. 4.8(b) and 4.8(c), respectively. Moreover, the absorptivity response is different for both TE and TM polarizations. This is due to the structure experiencing different free space impedances, as discussed in chapter 3.

4.3.2 Fabrication and experimental validation

To validate the simulation result, a porotype is fabricated with a size of

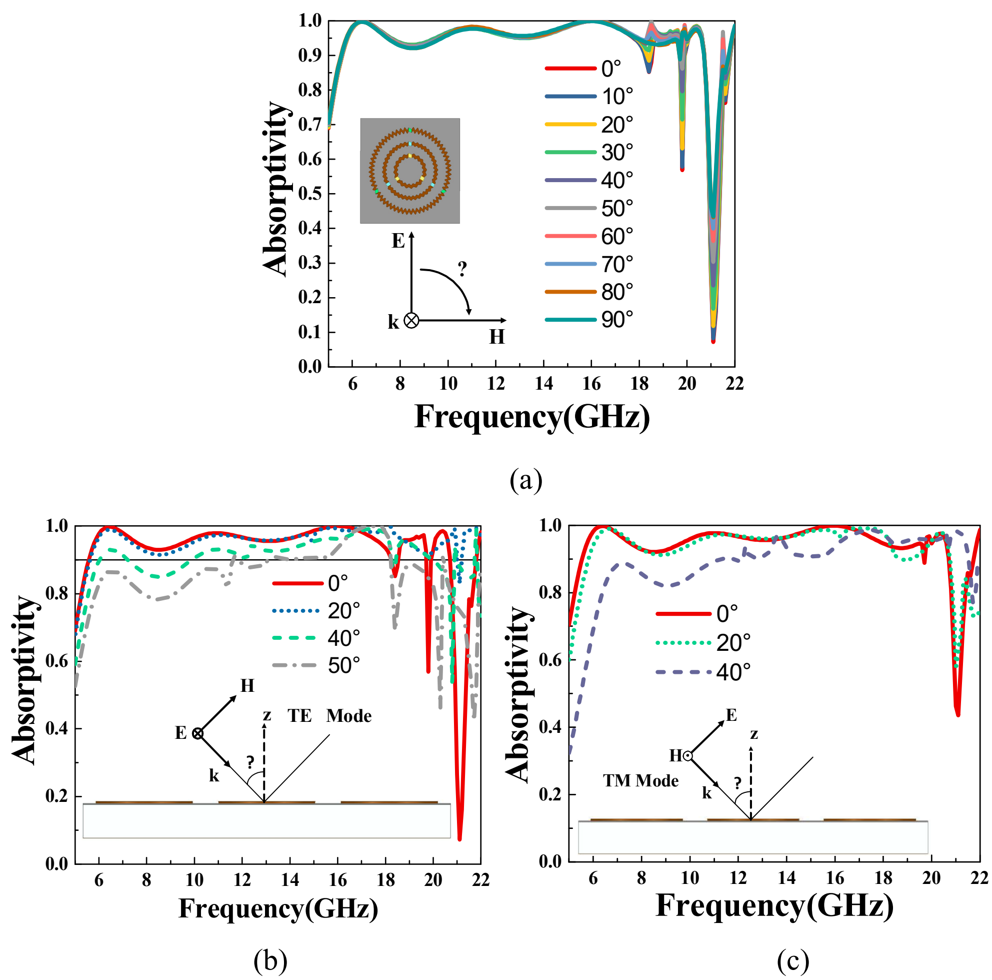

Fig. 4.8 (a) Electromagnetic absorption performance for different polarization angle (b) Electromagnetic absorption performance for oblique incidence under TE polarization. (c)Electromagnetic absorption performance for oblique incidence under TM polarization.

232.5×232.5 mm^2, as depicted in Fig. 4.9. The chip resistors of 100 Ω, 150 Ω, and 205 Ω with 1 % tolerance (ERJ2RKF1000X 1500X, 2050X from Panasonic) are soldered using surface mount technology. For both planar and conformal configurations, we employed the free-space measurement technique [89] to measure the co- and cross- polarized reflection properties, as shown in Fig. 4.10 (a) and 4.10 (b).

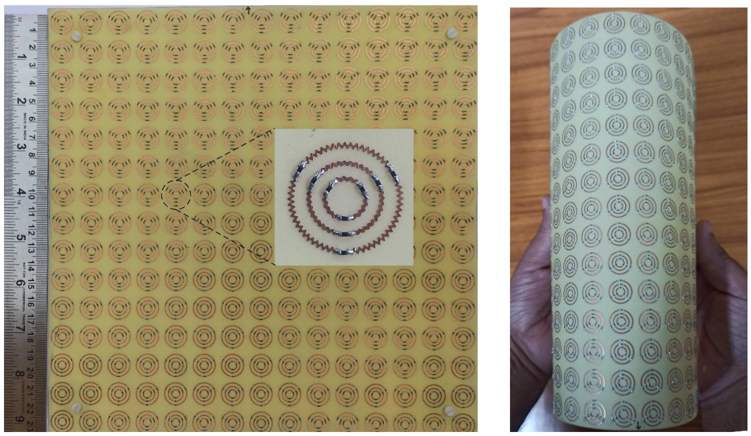

(a) (b)

(c) (d)

Fig. 4.9: (a) Image of fabricated absorber (b) Flexible top resistive metasurface used in our design (c) Measured thickness of fabricated conformal top resistive metasurface (d) Resistive metasurface combined with flexible foam.

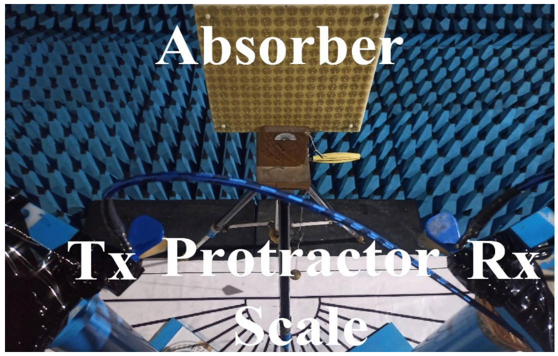

(a)

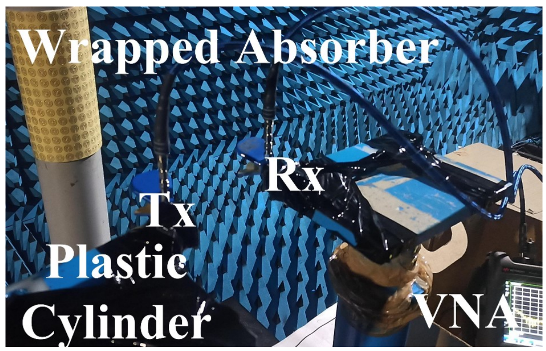

(b)

Fig. 4.10: (a) Measurement setup for planar absorber (b) Measurement setup for planar Conformal absorber

In the case of the planar absorber, under normal incidence, Fig. 4.11 illustrates the good consistency between measured and simulated results. However, small discrepancies arise between simulated and measured results due to measurement limitations such as finite sample size, the availability of time domain gating features, and fabrication tolerance.

In the case of validation for conformal application, absorptivity measurements are conducted by wrapping the planar absorber on cylindrical surfaces with different diameters, as shown in Fig. 4.11. From the result, it can be inferred that at certain points, absorption performance slightly deviated with the decrease in conformal radius. It happens because different areas of the bent absorber experience different oblique incidence, when a plane wave incident upon it.

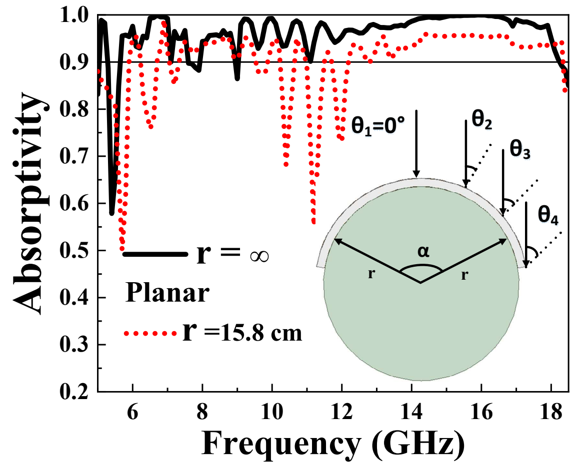

Fig. 4.11: Measured absorptivity at different bending radii.

TABLE 4.1
COMPARISON OF PROPOSED ABSORBER WITH REPORTED ABSORBER

Ref.	P mm (λ_L)	t mm (λ_L)	FBW (%)	F_D	CPRC	Unit cell configuration	R	φ_B
[51]	20 (0.14)	13 (0.09)	59.3	Difficult	No	3D Resistive FSS with vertical crisscross mesh	8	No
[55]	14 (0.25)	4.4 (0.078)	76.4	Easy	No	2 layer, Lossy FSS+ Lossy FSS	8	No
[121]	26 (0.33)	6.2 (0.079)	117	Difficult	No	3 layer, Lossy FSS+ Air Spacer +HIS	20	No
[49]	12.8 (0.33)	4 (0.098)	45	Difficult	No	3 layer, Lossy FSS+ Air Spacer +HIS	6	No
[56]	12.5 (0.28)	3 (0.067)	101.7	Easy	Yes	2 layer, Lossy FSS+ Air Spacer	8	No
[83]	14.4 (0.29)	3.68 (0.07)	72.8	Difficult	No	2 layer, Lossy FSS+Rubber Spacer	8	Yes
Pro.	**15.5 (0.28)**	**5.1 (0.09)**	**106.7**	**Easy**	**Yes**	Meandered rings embedded with lumped resistor + Air Spacer	9	**Yes**

λ_L: free space wavelength at the lowest operating frequency having absorptivity >90%, P: Periodicity, t: Thickness, FBW: Fractional Bandwidth, F_D: Design Flexibility to choose unit cell geometrical parameter as per limiting Frequency (lower and upper) of desire band along with some miniaturization aspect of the absorbing structure, CPRC: Cross-polarized reflected component, φ_B= Conformality alongwith Effect of Bend reported, HIS: High Impedance Surface

4.4 Conclusion

A low profile, conformal, ultra-wideband absorber with a low cross-polarization level has been designed and experimentally verified in this chapter.

The performance of the proposed absorber is compared with other reported wideband absorbers in Table 4.1. It can be observed that conformality with low cross polarization characteristic is achieved along with comparable numbers of lumped resistance and periodicity. Moreover, proposed absorber has highest fractional bandwidth (FBW), except [121]. But [121] has used 20 number of resistance per unit cell compared to we use 9 number of resistances. Although the reported works in [55], [121], [56], and [83] have a thinner unit cell dimension in comparison to the proposed work. However, these reported works either limited by rigid substrate or a lack of information regarding the cross-polarized reflected component.The proposed absorbr offers design flexibility for independent control over each resonant frequency and, consequently, on operating bandwidth, along with some miniaturized absorbing structure performance.The proposed structure has a low-profile configuration in terms of thickness, the number of layers, and lumped resistors while simultaneously achieving the characteristics mentioned in Table 4.1.

These are several important characteristics that make the proposed low profile efficient conformal absorber a promising candidtate in the field of modern wireless technology with practical application.